INTEGRATION, the VLSI journal 84 (2022) 142–150

Contents lists available at ScienceDirect

Integration, the VLSI Journal

journal homepage: www.elsevier.com/locate/vlsi

Very compact 3D-printed folded branch-line hybrid coupler based on loaded helical-microstrip transmission lines☆

A. Salas-Barenys *, N. Vidal, J.M. López-Villegas

Department of Electronics and Biomedical Engineering, Universitat de Barcelona, Barcelona, Spain

ARTICLE INFO

Keywords:
3D printing
Hybrid coupler
Compactness
Ultra high frequency band
Helical-microstrip transmission lines

ABSTRACT

This paper presents a 3D topology for high miniaturization of the well-known hybrid branch-line coupler at the UHF band. A preliminary work already proposed the use of helical-microstrip TLs combined with a folded structure for this purpose. This extended work includes a compactness enhancement by loading the TL segments with capacitors. An study of loaded helical-microstrip TL is reported as well. The coupler prototypes have been simulated and fabricated by using a combination of Additive Manufacturing and copper electroplating. The performance results have been compared to the conventional model showing a good agreement. In order to place the designed devices within the state of the art a figure of merit that combines the compactness and the relative bandwidth has been proposed, showing very good results in terms of miniaturization.

1. Introduction

Hybrid couplers are crucial devices for some HF, VHF and UHF applications such as quadrature combining or power division. Fig. 1 shows the topology of a traditional branch-line hybrid coupler, which is based on a square with two parallel TL of a characteristic impedance Z_0 that are perpendicular to the two other transmission lines of $Z_0/\sqrt{2}$ [1]. The dimensions of these devices are constrained by the signal wavelength, that implies a considerable size problem for these range of frequencies that can go from few kHz to hundreds of MHz. For that reason, there are many contributions to the topic with different miniaturization techniques, using (e.g) lumped elements [2], discontinuous microstrip lines [3], metamaterials [4] or shunt capacitors [5,6].

Hereon, Additive Manufacturing (AM) appears, as an alternative solution for the miniaturization of these kind of devices by the use of full 3D-space design. The use of 3D printed electronics has been proved in former works by developing a manufacturing technology based on a combination of AM and copper electroless plating [7–9]. A preliminary work [10] explained, two different techniques that can be applied to compact the conventional structure of an hybrid coupler: the first one consists of the implementation of a helical shape for the TL segments, that has been studied in former works [11,12]. The second transformation folds the planar structure by the square diagonals, resulting in a more compacted 3D topology. Finally, this current paper explores a new step that takes profit of the existing surfaces to load the TLs with capacitances in order to enlarge their electrical path, as in [5,6].

Henceforth, this work presents a compactness enhancement for hybrid couplers based on capacitive loading of the helical-microstrip TL segments. The folded coupler concept is explained in Section 2. The loading improvement is then described in 3 together with a study and modeling of the compactness dependence with the capacitor surface. For comparison purposes, three different prototypes have been designed: a planar coupler following the traditional topology, which is labeled HYB_t, a folded coupler based on helical-microstrip TL and labeled HYB_F and, finally, the new prototype based on HYB_F with capacitor loads and labeled HYB_{FL}. The simulation results and the dimensions of each model are presented in Section 4. Then, the manufacturing process is briefly commented in Section 5. Section 6 is used for discussion of the experimental results. The compactness achievements are compared there against some works within the SoA as a proof of concept. The conclusions are presented in Section 7.

2. 3D-folded hybrid coupler

A deep study on helical-microstrip TLs can be found in this former work [12], where their compactness implications and limitations were demonstrated and discussed. As told, the first topology implementation consists of substituting the conventional planar microstrip TL segments for this kind of helical-shaped lines, whose CAD mode is depicted in Fig. 2. The second transformation folds the square structure following the sequence in Fig. 3. During the first step, in Fig. 3a, the square is

☆ This work was supported in part by the Spanish Secretary of State for Research, Development and Innovation Under Project TEC2017-83524-R.
* Corresponding author.
E-mail addresses: arnau.salas@ub.edu (A. Salas-Barenys), nvidal@ub.edu (N. Vidal), j.m.lopez_villegas@ub.edu (J.M. López-Villegas).

https://doi.org/10.1016/j.vlsi.2022.02.001
Received 12 February 2021; Received in revised form 20 September 2021; Accepted 2 February 2022
Available online 12 February 2022

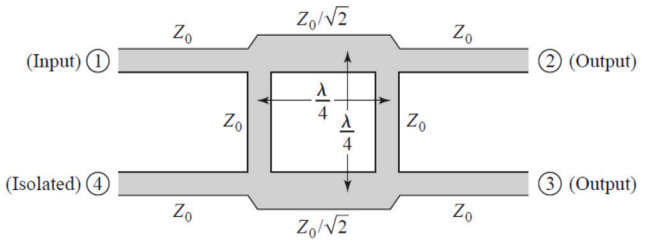

Fig. 1. Conventional topology of a quadrature hybrid coupler. Picture extracted from [1].

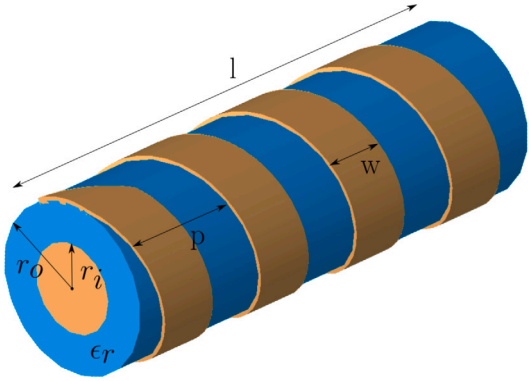

Fig. 2. CAD model of a helical-microstrip TL.

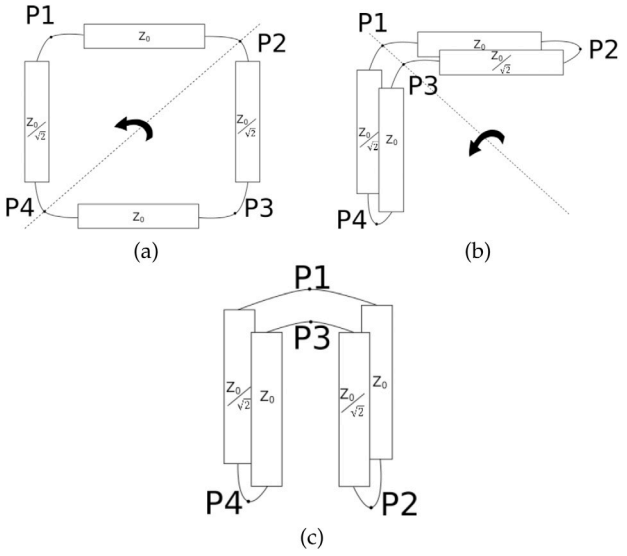

Fig. 3. Design steps for the global structure of the proposed hybrid coupler.

folded by the first diagonal, moving the port 3 towards the port 1. The result and the next step are depicted in Fig. 3b, where the structure is folded again by the other diagonal of the original square, moving the port 2 towards the port 4. The final topology is shown in Fig. 3c and the four TL segments are all placed in parallel.

According to the schematic of Fig. 3, the lines could be as close to each other as desired. That is not true in practice for two main reasons. The first one refers to the requirements of the manufacturing process, that will be summarized latter. The other one would be related to the electromagnetic coupling between lines, although, that will be out of concern, considering the spacing set due to the first reason.

The connection between lines and ports is represented in Fig. 3 by wires. The HYB_F prototype uses planar microstrip TLs to perform

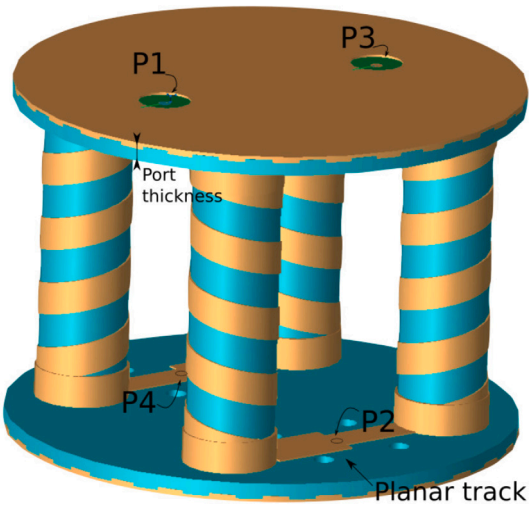

Fig. 4. CAD model of the HYB_F folded hybrid branch-line coupler based on helical-microstrip TL.

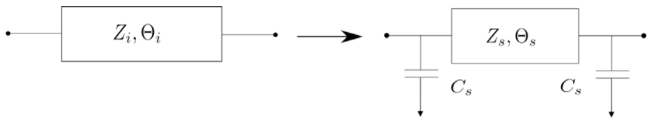

Fig. 5. Model of the equivalent of a pure transmission line with a loaded transmission line.

this function. This is illustrated in the CAD model of Fig. 4, where the helical lines are placed in circular symmetry. They are held by a thin disk at each side, that play the roll of substrate for the planar TLs, as well.

The disk (or port) thickness is set to the minimum permitted by the manufacturing process. The desired characteristic impedance of the planar segments is then found by changing the track width. In the case of the helical lines, the width, the outer radius and the pitch have been fixed thus the characteristic impedance is found by changing the inner radius. The length of the electrical path is adjusted by the cylinder length. The rings at each side of the cylinders are used to ensure a proper connection between helical and planar TLs. Ports are surrounded by holes to hold the screws for the attachment of the SubMiniature version A (SMA) connectors.

3. Loaded TLs

Loading transmission lines with capacitors is a common way for size reduction [6]. This is based on the theory that any transmission line of characteristic impedance Z_i and phase Θ_i might be decomposed in a shorter line of Z_s and Θ_s loaded with capacitors of capacitance C_s at both sides. This equivalence is depicted in Fig. 5.

Taking back a look at Fig. 4, it can be seen that these extra capacitors can be easily added by plating the inner face of the disk. By this way, the new component is integrated without requiring neither more surface nor more volume, but making use of the already existing. In order to simplify the design, this disk will now be a squared sheet. Therefore, the resultant loaded helical-microstrip TL will be like that in Fig. 6, where the external faces of the squares are connected to the inner conductor. Hence, the load capacitance value can be calculated as that between two squared parallel planes with edge a after subtracting the area of a circle of radius r_o.

$$C_s = \epsilon \frac{(a^2 - \pi r_o^2)}{t}, \tag{1}$$

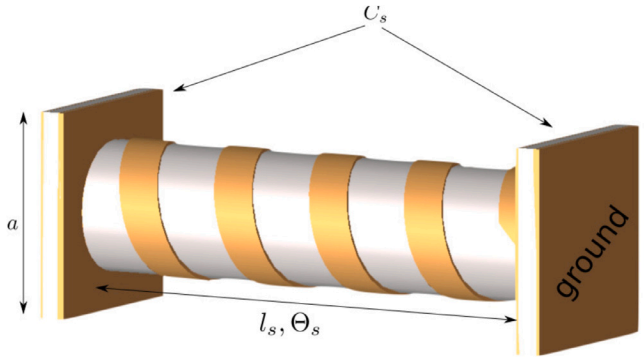

Fig. 6. CAD model of a loaded helical-microstrip TL.

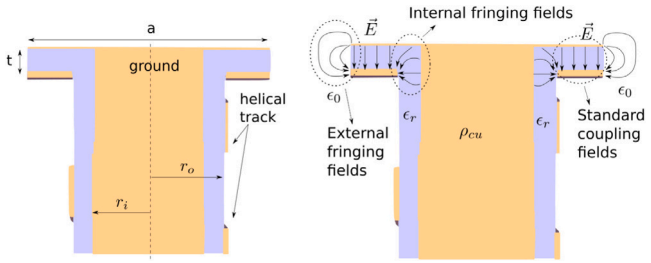

Fig. 7. Vertical cross section of the loaded helical-TL segment with dimensions (left) and with the load standard and fringing fields representation (right).

where t is the thickness of the planar substrate or the distance between plates and ϵ is the dielectric constant. It is worth to notice that this is an ideal approximation that does not take in account the fringing effects, although it will still be useful as a first approach.

The equivalence in Fig. 5 can be algebraically modeled by means of the ABCD parameters [6], from which the following expression can be obtained

$$2\pi f_0 C_s = \frac{\cos\Theta_s - \cos\Theta_i}{Z_i \sin\Theta_i}, \tag{2}$$

where f_0 is the work frequency. The loaded transmission line must be sized to have a quarter-wavelength phase while actual line should be shorter, thus it can be assumed that $0 \leq \Theta_s \leq \Theta_i = \pi/2$. The phase of any line can now be considered as

$$\Theta = \frac{2\pi l_e}{\lambda_0}, \tag{3}$$

being λ_0 the wavelength related to the work frequency. Thus, considering that $\Theta_i = \pi/2$

$$l_{e_i} = \frac{\lambda_0}{4} = \frac{c_0}{4f_0}, \tag{4}$$

where c_0 is the speed of light. Then, combining (2)–(4) and rearranging gives

$$l_{e_i} = \frac{\pi}{2}\frac{Z_i C_s c_0}{\cos\Theta_s}. \tag{5}$$

According to (3) and (4), the phase shift of the loaded segment can be described by

$$\Theta_s = \frac{\pi}{2}\frac{l_{e_s}}{l_{e_i}}, \tag{6}$$

Henceforth, the cosine in (5) can be simplified by

$$\begin{aligned}\cos\Theta_s &= \cos\left(\frac{\pi}{2}\frac{l_{e_s}}{l_{e_i}}\right) = \cos\left(\frac{\pi}{2} - \alpha\right)\\ &= \sin\alpha \approx \alpha = \frac{\pi}{2}\left(1 - \frac{l_{e_s}}{l_{e_i}}\right),\end{aligned} \tag{7}$$

where the sine approximation is valid for small values of the angle α. That can be assumed for high values of the ratio $\frac{l_{e_s}}{l_{e_i}}$, which is always less than 1, since $l_{e_s} < l_{e_i}$. Substituting, now, the cosine approximation in (5) gives that

$$l_{e_i} \approx Z_i C_s c_0 + l_{e_s}. \tag{8}$$

The approach of (8) can be improved if taking in account the fringing fields of the load capacitors. Fig. 7 shows the different electric coupling fields of concern. Using (1) to calculate C_s only considers the standard fields, which are those uniform and perpendicular to the capacitor electrodes.

The fringing fields have been divided in two types: the external ones, whose lines travel across the air (ϵ_0-medium), and the internal ones, whose lines travel across the dielectric substrate (ϵ_r-medium). The effect of the concerning phenomenon can be approached by an increment of the resultant capacitance from respect the standard capacitor. This increment can be found by a conformal mapping transformation and then integrating the electrostatic fields, where, the results will be different depending on the approximations applied [13–16]. The approximation chosen is the one that has provided better accuracy comparing to the simulations, which is that proposed by Sloggett [16]. Then, the effect of the external fringing fields can be modeled by an extra capacitor with air as dielectric medium such as

$$C_f \approx \frac{C_s}{\epsilon_r}\frac{2t}{\pi R}\ln\frac{e\pi R}{t}, \tag{9}$$

where e is the Euler's number, ϵ_r is the relative permittivity of the substrate and R is the radius of a circular parallel plate capacitor. According to the principle of equal area [13], R can be approximated to

$$R \approx \sqrt{\frac{a^2}{\pi}}. \tag{10}$$

Finally, the achieved electrical length as a function of the load capacitor taking in account the effect of the external fringing can be described by

$$l_{e_i} \approx Z_i(C_s + C_f)c_0 + l_{e_s}. \tag{11}$$

That expression permits to predict by an approximation the expected compactness of loaded TLs l_{e_i}/l. In order to do that, it must be used the expression of the electrical length of a helical-microstrip TL demonstrated in a former work [11].

In order to verify the model in (11), a set of 10 loaded helical-microstrip TL samples have been designed with a sweep over the capacitor edge a and their electromagnetic behavior have been simulated within the EMPro environment. Each sample has been set to have a characteristic impedance as close as possible to $Z_i = 50\ \Omega$ at the same frequency where the phase shift is $\phi_{21} = \pi/2$. To ensure that, r_i and w have been accordingly modified, while the parameters l, r_o and p have been respectively fixed to 25, 3 and 5 mm. The thickness of the load capacitor is minimized to $t = 1$ mm in order to increase the capacitance density. The experimental electrical length is then extracted by using

$$l_e = -\frac{c_0}{2\pi}\frac{\phi_{21}}{f}. \tag{12}$$

The comparison between the theoretical results and the data obtained by the simulations, which present a considerable agreement, is depicted in Fig. 8. As expected, the compactness is incremented if considering the external fringing fields, since the total capacitance is higher than only taking in account the conventional one. Nevertheless, it can be seen than the computed simulations give even a higher level of the ratio l_{e_i}/l because of the effect of the internal fringing fields. This discrepancy is reduced for larger capacitors, since the internal fringing

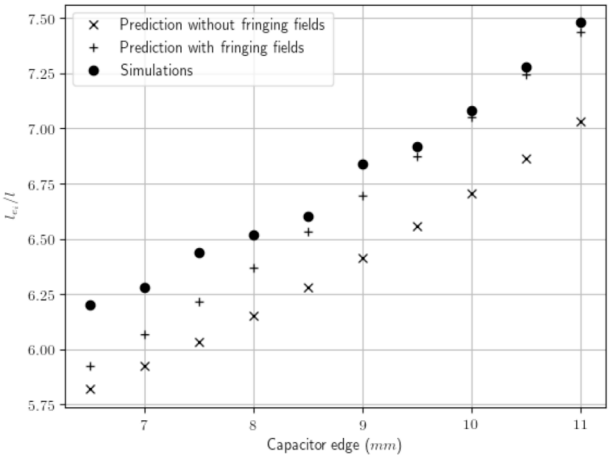

Fig. 8. Compactness of loaded helical-microstrip TL segments as a function of the capacitor edge size. Comparison between the simulations and the theoretical prediction with and without considering the fringing effect.

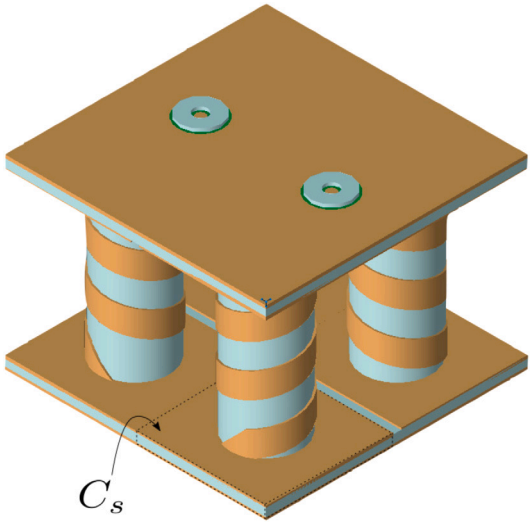

Fig. 9. Model of the HYB_{FL} folded hybrid branch-line coupler with loaded helical microstrip transmission lines.

fields become less significant from respect the other fields (both the surface and the external perimeter grow).

Probably, the major setback of loaded transmission lines is the reduction of the available bandwidth. Nevertheless, this limitation is not particularly relevant in this work, since a branch-line hybrid coupler has already a narrow response. This will be demonstrated in the simulations and measures of the prototype with loaded helical-microstrip TL segments. Moreover, a FoM relating the relative bandwidth and the compactness is presented below in the experimental measure section for comparing with the traditional topology and other works found within the SoA.

The CAD model proposed for the folded hybrid branch-line coupler with loaded helical microstrip transmission lines is labeled HYB_{FL} and presented in Fig. 9. It can be seen that it is basically based on the unloaded prototype making use of the already existing support surface to implement plane-parallel plate capacitors as C_s. Contiguous capacitors are joined all along one edge, ensuring a better connection between them and also between adjacent lines.

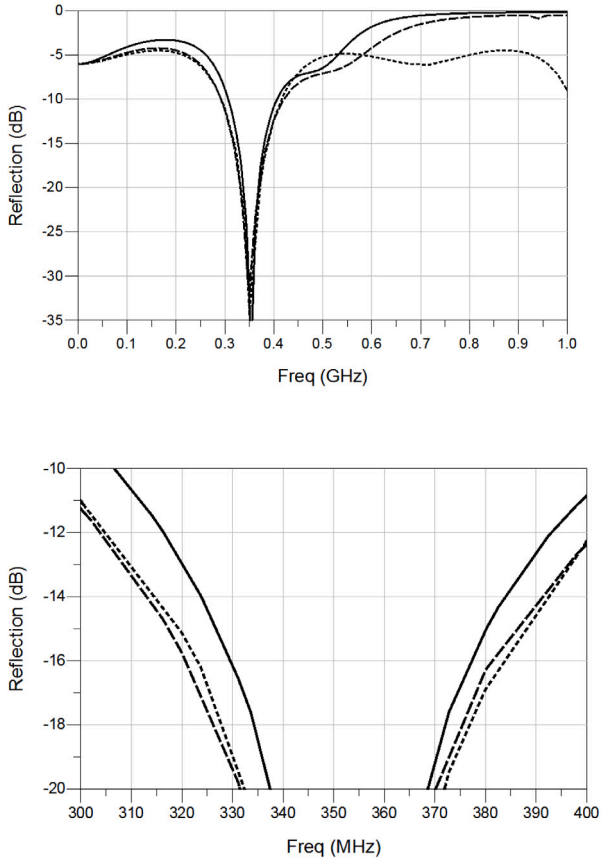

Fig. 10. Simulation results of the reflection coefficient for the traditional (···), the unloaded (- - -) and the loaded (—) prototypes.

Table 1
Dimensions in mm of the coupler prototypes that have been designed and fabricated.

Dimension (mm) \Prototype	HYB_t	HYB_F	HYB_{FL}
Length (50 Ω-line)	117.5	30	20
Length (35.36 Ω-line)	114.6	30	20
Planar substrate thickness	1.57	1.5	1
Pitch (50 Ω-line)	–	6.1	6
Pitch (35.36 Ω-line)	–	6.2	6
External cylinder radius	–	4	4
Inner cylinder radius (50 Ω-line)	–	2.4	2.05
Inner cylinder radius (35.36 Ω-line)	–	3	2.92
Planar track width (50 Ω-line)	3.1	3.3	–
Planar track width (35.36 Ω-line)	5.1	5.7	–
Helical track width	–	3	3
Loading capacitor edge	–	–	8
Board length	134.6	–	–
Board width	142.3	–	–
Supporting board diameter/length	–	24	16
3D coupler total length	–	33	22

4. Simulation data

The CAD models have been designed for proper electromagnetic simulation, including a coupler with the traditional topology of Fig. 1 and labeled HYB_t. In the case of this conventional coupler, the CAD model has been carried out using the Momentum tool of the ADS environment software, from Keysight. The EMPro software has been used for the 3D prototypes instead. The chosen substrate material for the different devices are the following:

- HYB_t: FR4 ($\epsilon_r = 4.7$, $\tan\delta = 0.014$)
- HYB_F: Therma 294 ($\epsilon_r = 3.1$, $\tan\delta = 0.025$)
- HYB_{FL}: High Temp ($\epsilon_r = 2.8$, $\tan\delta = 0.021$)

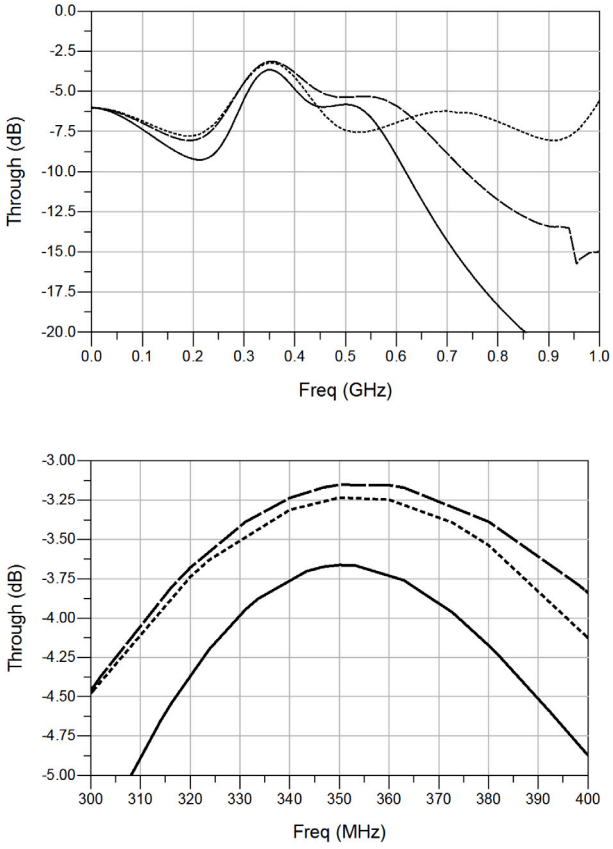

Fig. 11. Simulation results of the through coefficient for the traditional (···), the unloaded (- - -) and the loaded (—) prototypes.

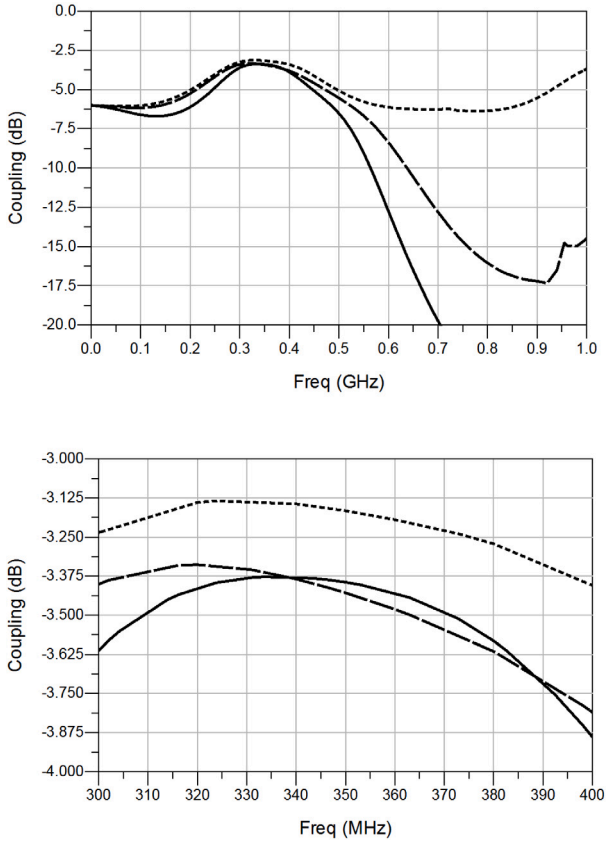

Fig. 12. Simulation results of the coupling coefficient for the traditional (···), the unloaded (- - -) and the loaded (—) prototypes.

The reason of choosing a material with lower permittivity for the loaded prototype comes from considering the manufacturing process and that the printer using High Temp (Objet 260 Connex 1, from Stratasys) is more precise than the one using Therma 294 (XFAB, from DWSystems).

After integrating the four segments for the design of a coupler, the dimensions have to be adjusted to find the parameters that better fit the desired specifications. The final values for all the branch-line couplers, centered at 350 MHz, are listed in Table 1. The supporting board refers to the substrate sheet that holds the helical lines in the 3D prototypes. The dimension is named diameter for the HYB_F (circular board) and length for the HYB_{FL} (squared board). The coupler total length comes from the sum of cylinder length and twice the planar substrate thickness. These parameters will be useful for the calculation of the occupied area in single plane in the experimental measure section.

Both 3D prototypes have been compared to the traditional coupler with respect to the scattering parameters. The reflection coefficient is presented in Fig. 10 where it can be seen that it goes below −30 dB for all models. HYB_{FL} has a minimum of −35 dB and a very small discrepancy in the frequency of work, below a 3% of relative deviation. In the zoomed window it can proved that there is no reduction of the bandwidth in loading the transmission lines with capacitors since all three prototypes have about 10% of relative bandwidth.

Looking at the other parameters, such as the Through at Fig. 11, the Coupling at Fig. 12 and the Isolation at Fig. 13, it can be seen that both miniaturized prototype models are in good agreement with the response of the conventional coupler.

5. Manufacturing process

The three types of couplers have been manufactured by different technologies to work at the same frequency of 350 MHz. The HYB_t by the use of a standard-Printed Circuit Board (PCB) technique on a FR4 substrate. The HYB_F has been printed with the XFAB machine from DWS Systems based on stereolithography and using Therma 294 as dielectric base material. On the other hand, the HYB_{FL} has been printed with the Objet 260 Connex 1 based on material jetting and using High Temp as dielectric base material. Both 3D prototypes have been metallized by the use of copper electroplating. The full manufacturing process has already been discussed in former works [7,8]. This 3D-printed electronics manufacturing technology is very new and should not be compared to a conventional process in terms of cost and efficiency. In order to do that, the presented technology should be fully optimized and automated.

6. Experimental measures

A picture of the final prototypes is presented in Fig. 14, where the miniaturization enhancement of both 3D couplers against the conventional one appears very clear. Since the devices have different shapes, it has been taken as size reference the cross section of each device while it is orientated along the plane that is parallel to the SMA connector direction. The area of this final section S_f can be then calculated using the parameters in Table 1. In the case of HYB_t, S_f is obtained by multiplying the board length by the board width. On the other hand the HYB_F prototype S_f comes from multiplying the coupler total length by the supporting board diameter, while in the case of the HYB_{FL} it comes from the product of the total length and the supporting board length. The results are listed in Table 2.

Hereon, let the relative compactness be defined as the ratio between the S_f of the traditional coupler and the S_f of the evaluated

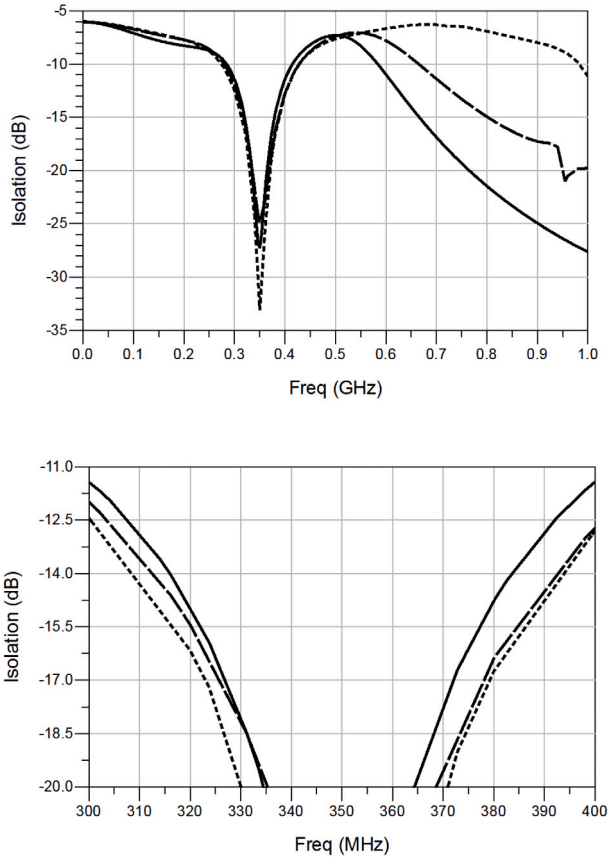

Fig. 13. Simulation results of the isolation coefficient for the traditional (···), the unloaded (- - -) and the loaded (—) prototypes.

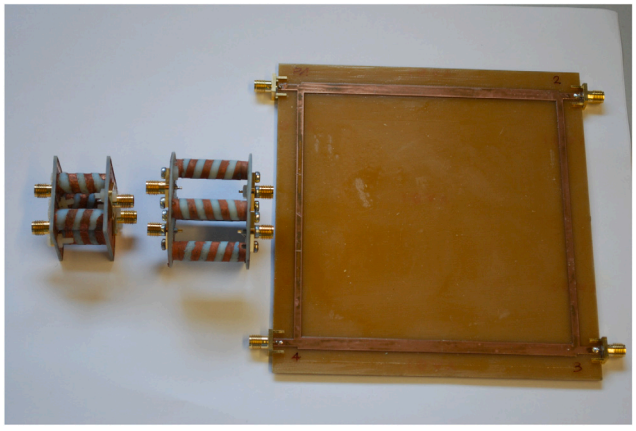

Fig. 14. Hybrid branch-line coupler prototypes. From left to right, HYB_{FL}, HYB_F and HYB_t.

Table 2
Occupied surface by the 3D-printed hybrid coupler prototypes.

Prototype	S_f (cm^2)
HYB_t	191.54
HYB_F	7.68
HYB_{FL}	3.52

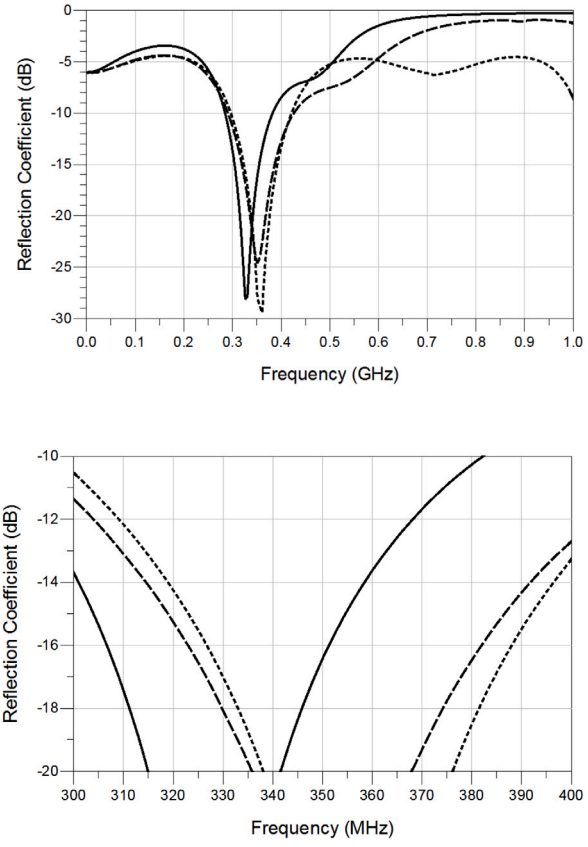

Fig. 15. Measurement data of the reflection coefficient for the traditional (···), the unloaded (- - -) and the loaded (—) prototypes.

device. Therefore, the more the section of the proposed prototype is miniaturized, the higher the level of compactness becomes.

$$Compactness = \frac{S_{f_{traditional}}}{S_{f_{prototype}}} \tag{13}$$

According to this definition, the HYB_F and the HYB_{FL} compactness respectively correspond to 24.9 and 54.4. It can be noticed that the dielectric constant of FR4 is higher than that of Therma 294 used for the HYB_F, which is still higher than the one of High Temp used for HYB_{FL}. A high permittivity implies a slower phase velocity and thus a larger electrical length, thus the final relative miniaturization would be even more if the same substrate material had been used for all the samples.

The characterization of the manufactured prototypes has been carried out with a 4-port E5071C Vector Network Analyzer (VNA) from Keysight Technologies Inc. Figs. 15–18 respectively show the measured reflection, through, coupling and isolation coefficient responses of the manufactured prototypes. Comparing to Figs. 10–13 can be seen that the measured scattering parameters are in good agreement with the simulation data.

Looking at the reflection coefficient in Fig. 15, the HYB_F prototype goes down to −25 dB while the HYB_{FL} to less than −28 dB, that is very close to the −29 dB of the planar structure. On the other hand the work frequency relative deviation from the ideal response is higher for the HYB_{FL} prototype, being 5.7%, than for the HYB_F, which is 0.3%. Therefore, the used 3D manufacturing process gives satisfactory result even in comparison with the HYB_t PCB technology, that led to a frequency relative deviation of 2.9%. In Fig. 15, the bandwidth can also be observed, and, as expected, the decrement of the 3D models is not very significant, since the conventional design already performs a narrow response. The measured relative bandwidth related to −20 dB

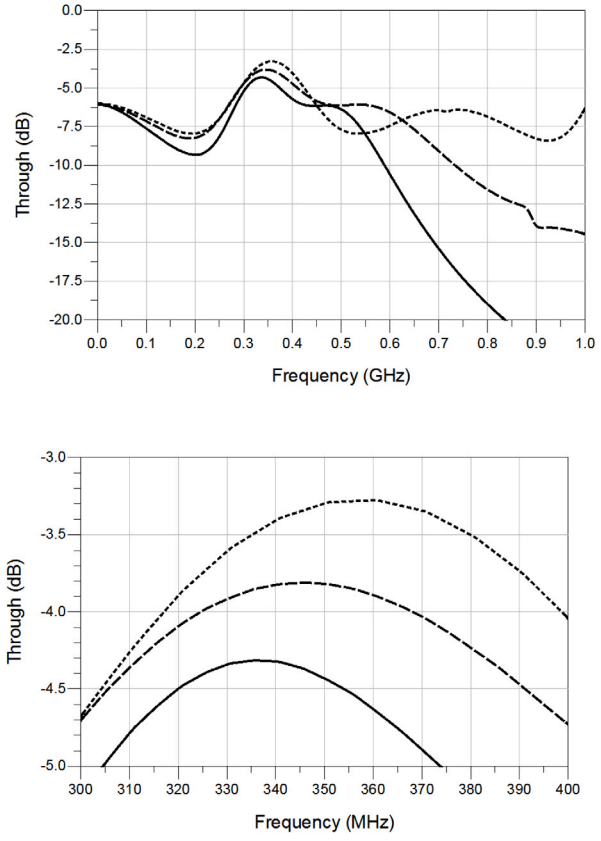

Fig. 16. Measurement data of the through coefficient for the traditional (···), the unloaded (- - -) and the loaded (—) prototypes.

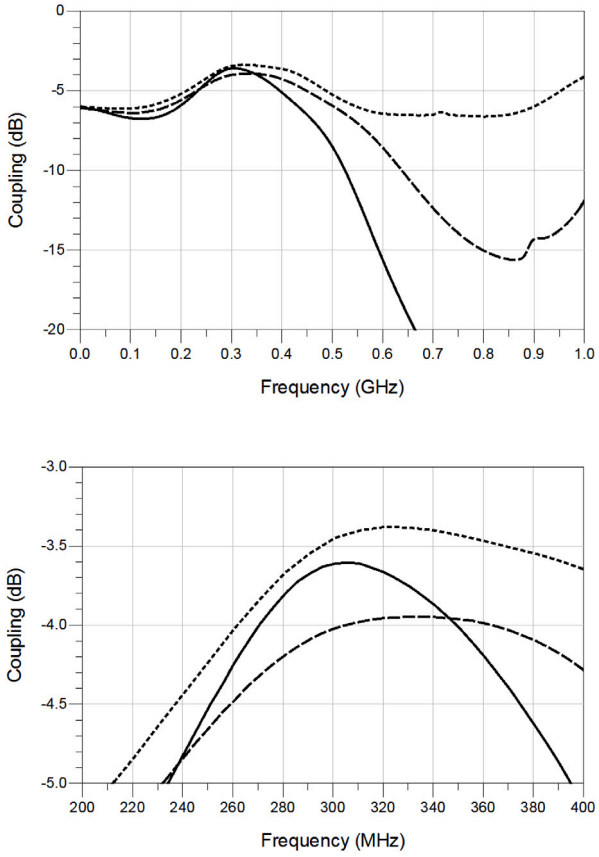

Fig. 17. Measurement data of the coupling coefficient for the traditional (···), the unloaded (- - -) and the loaded (—) prototypes.

of return loss have been found to be 10.9, 8.9 and 7.7% for the HYB_t, HYB_F and HYB_{FL} prototypes, respectively.

Fig. 16 shows the through coefficient. Considering that the ideal output is of −3 dB, the measured insertion loss is −0.28, −0.81 and −1.32 dB for the planar, unloaded and loaded prototypes, respectively. The 3D models are more lossy due to the discrepancies between the metallization results and bulk copper conductivity. That is also supported by comparing the total normalized scattered power on each device given by the expression

$$Power_S = S_{11}^2 + S_{21}^2 + S_{31}^2 + S_{41}^2. \tag{14}$$

The use of the normalized parameters forces the power to go from 0 to 1 in passive networks, being normal to the power of the exciting signal. This information is depicted in Fig. 19. The difference between 1 and the summation in (14) means either dissipated or radiated power.

Figs. 17 and 18 are related to the coupling and a isolation coefficients. The results are very similar to the through and reflection coefficients, respectively.

For some hybrid coupler applications it is important to ensure the quadrature (±90 degrees shift) between both output ports at the work frequency. This phase difference is depicted in Fig. 20, where the quadrature occurs close to the work frequency for all the devices. The higher discrepancy is 6.4° from the expected response and is performed by the HYB_{FL}. Considering that the work frequency of this prototype is shifted down to 330 MHz, the error is reduced to 3.6°.

Another way to compare the prototypes is by the use of a FoM that combines the aforementioned compactness, defined in (13), and the relative bandwidth. This is represented in Fig. 21. The bandwidth is relative to the center frequency of the corresponding device. Hereon, the best expected performance of a coupler would be on the right-upper corner of the plot, which would mean a high level of compactness and a large bandwidth. According to this figure, the proposed 3D models are very interesting, since they achieve a high level of compactness without loosing significant bandwidth spectrum. Other improved prototypes using planar technology have been included in the same plot in order to compare the obtained results with the SoA. This comparison should be understood as a proof of concept since each device use a manufacturing technology in different stages of development; use different substrate base materials and is designed at a different center frequency. Only devices that work at the VHF or the UHF bands have been taken as samples. In order to better compare the presented references with the current work, Table 3 shows their compactness, center frequency f_o, relative bandwidth, type of coupler and the used technique for miniaturization. Some of the other authors' information related to the bandwidth is approximated, since not all the data is explicitly given.

It can be seen that [6] provides an important enhancement regarding the bandwidth and [21] and interesting trade-off between compactness and bandwidth. However, none of the found devices achieves the level of compactness reached by the HYB_{FL} model presented in the current paper.

7. Conclusions

As a summary, in this work two new designs of 3D branch-line couplers have been presented. The first one (HYB_F) consists of the application of helical-microstrip TL segments and a folded structure for miniaturization. The second one (HYB_{FL}) improves the final compactness by including capacitor loads at both side of the TL segments. A study on loaded helical-microstrip TL segments has been carried out, showing that the compactness achieved goes in detriment of the

Table 3
Comparison table of presented devices against the conventional hybrid coupler and other works find within the SoA. The sixth column refers to the type of coupler, where BL stands for branch-line and RR for rat-race. Some of the information related to the bandwidth from the other authors is approximated, since not all the data is explicitly given.

Ref	Compactness	f_0 (MHz)	BW (%)	ϵ_r	Coupler	Technique
HYB_t	1.00	350	10.9	4.7	BL	Conventional
Sun [3]	2.44	1000	10	2.2	BL	Discontinuous microstrip Lines
Tsai [5]	3.73	836.5	3.6	4.2	BL	Load capacitors
Chun [6]	2.20	2000	56	3.05	BL	Load capacitors
Hung [17]	3.19	1000	3	4.4	BL	Artificial lines
Letavin [18]	4.46	900	7	4.4	BL	U-shaped capacitor
Velidi [19]	2.25	1000	9	4.3	BL	Signal-interference
Koziel [20]	8.06	1000	8	3.5	BL	Pattern search algorithm optimization
Kulkarni [21]	29.41	260	28.9	2.1	RR	Coaxial waveguide
HYB_F	24.90	350	8.9	3.1	BL	3D Folded structure
HYB_{FL}	54.40	350	7.7	2.8	BL	3D Folded structure and loaded capacitors

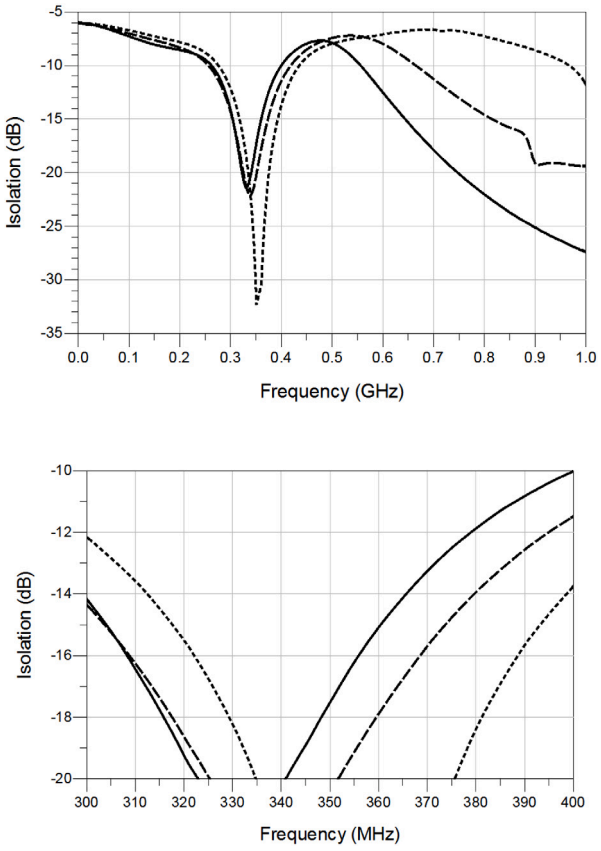

Fig. 18. Measurement data of the isolation coefficient for the traditional (···), the unloaded (- - -) and the loaded (—) prototypes.

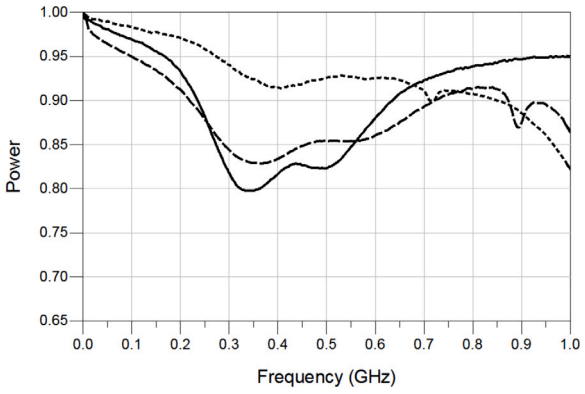

Fig. 19. Measurement data the scattered power for the traditional (···), the unloaded (- - -) and the loaded (—) prototypes. The power in the y axis is normalized by the power of the exciting signal.

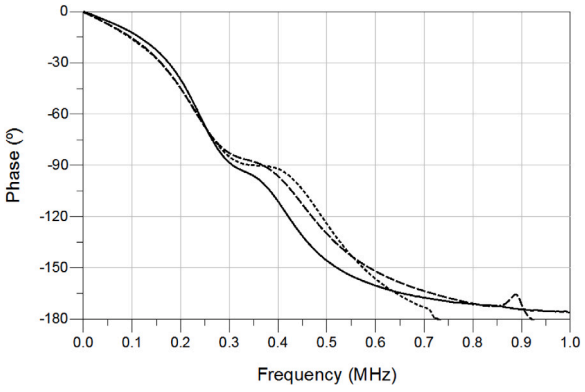

Fig. 20. Difference between the measured phase shift of the through and coupled ports for the traditional (···), the unloaded (- - -) and the loaded (—) prototypes.

available bandwidth. The simulations and the experimental measures present a good agreement. The prototypes have been compared to a conventional planar hybrid coupler (HYB_t) and other works within the SoA, showing a very high level of compactness, while the bandwidth limitation has not resulted a big concern since the planar structure already has a narrow spectrum.

Even thought the bandwidth reduction of the proposed models from respect the conventional structure is not very significant, it is still an important limitation. There can be found some solutions within the literature, such as cascading different couplers or using high impedance lines [6]. Future work would include developing other designs that enhance this feature and what are the singular possibilities that the three-dimensional space can offer.

CRediT authorship contribution statement

A. Salas-Barenys: Conceptualization, Methodology, Software, Validation, Formal analysis, Investigation, Data curation, Writing – original draft, Visualization. **N. Vidal:** Conceptualization, Investigation, Project administration, Funding acquisition. **J.M. López-Villegas:** Conceptualization, Methodology, Validation, Investigation, Writing – review & editing, Supervision, Project administration, Funding acquisition.

Declaration of competing interest

The authors declare that they have no known competing financial interests or personal relationships that could have appeared to influence the work reported in this paper.

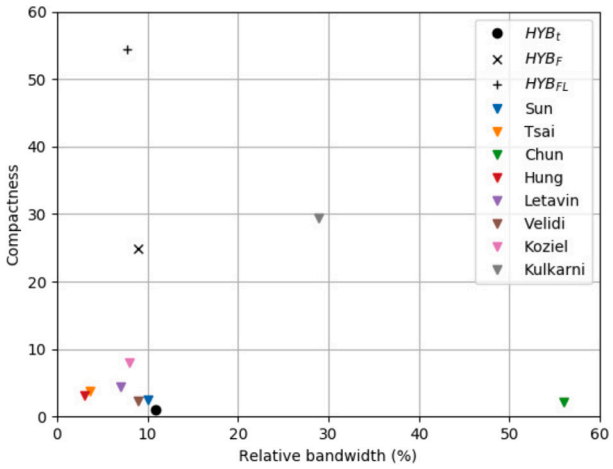

Fig. 21. FoM that relates the compactness defined in (13) with relative bandwidth of the presented prototypes, the conventional structure and some works found in the SoA. The bandwidth is relative to the work frequency of each device. The works from SoA are labeled with the name of the first author and are referred to [3,5,6,17–21].

References

[1] D. Pozar, Microwave Engineering, fourth ed., Wiley, 2011, [Online]. Available: https://books.google.es/books?id=JegbAAAAQBAJ.

[2] Z.J. Hou, L. Chiu, Q. Xue, A class of quadrature couplers based on transformer, IEEE Trans. Microw. Theory Tech. 64 (3) (2016) 785–797, http://dx.doi.org/10.1109/TMTT.2016.2519019.

[3] K.-O. Sun, S.-J. Ho, C.-C. Yen, D. van der Weide, A compact branch-line coupler using discontinuous microstrip lines, IEEE Microw. Wirel. Compon. Lett. 15 (8) (2005) 519–520, http://dx.doi.org/10.1109/LMWC.2005.852789.

[4] J. Bonache, G. Siso, M. Gil, A. Iniesta, J. Garcia-Rincon, F. Martin, Application of composite right/left handed (CRLH) transmission lines based on complementary split ring resonators (CSRRs) to the design of dual-band microwave components, IEEE Microw. Wirel. Compon. Lett. 18 (8) (2008) 524–526, http://dx.doi.org/10.1109/LMWC.2008.2001011.

[5] K. Tsai, H. Yang, J. Chen, Y.E. Chen, A miniaturized 3 db branch-line hybrid coupler with harmonics suppression, IEEE Microw. Wirel. Compon. Lett. 21 (10) (2011) 537–539, http://dx.doi.org/10.1109/LMWC.2011.2164901.

[6] Y.-H. Chun, J.-S. Hong, Compact wide-band branch-line hybrids, IEEE Trans. Microw. Theory Tech. 54 (2) (2006) 704–709, http://dx.doi.org/10.1109/TMTT.2005.862657.

[7] A. Salas-Barenys, N. Vidal, J. Sieiro, J.M. López-Villegas, B. Medina-Rodriguez, F.M. Ramos, Full-3D printed electronics process using stereolitography and electroless plating, in: 2017 32nd Conference on Design of Circuits and Integrated Systems (DCIS), 2017, pp. 1–4, http://dx.doi.org/10.1109/DCIS.2017.8311624.

[8] A. Salas-Barenys, N. Vidal, J. Sieiro, J.M. López-Villegas, B. Medina-Rodríguez, F.M. Ramos, Fabrication of full-3D printed electronics RF passive components and circuits, in: 2018 14th Conference on Ph.D. Research in Microelectronics and Electronics (PRIME), 2018, pp. 265–268, http://dx.doi.org/10.1109/PRIME.2018.8430356.

[9] J.M. Lopez-Villegas, N. Vidal, J. Sieiro, A. Salas, B. Medina, F.M. Ramos, Study of 3-D printed conical inductors for broadband RF applications, IEEE Trans. Microw. Theory Tech. (ISSN: 0018-9480) 66 (8) (2018) 3597–3602, http://dx.doi.org/10.1109/TMTT.2018.2845862.

[10] A. Salas-Barenys, N. Vidal, J.M. López-Villegas, Compact 3D-printed folded branch-line hybrid coupler based on helical-microstrip transmission lines, in: 2020 XXXV Conference on Design of Circuits and Integrated Systems (DCIS), 2020, pp. 1–5, http://dx.doi.org/10.1109/DCIS51330.2020.9268661.

[11] J.M. Lopez-Villegas, A. Salas, N. Vidal, Modeling of 3-d-printed helical-microstrip transmission lines for rf applications, IEEE Trans. Microw. Theory Tech. (ISSN: 1557-9670) 67 (12) (2019) 4914–4921, http://dx.doi.org/10.1109/TMTT.2019.2949312.

[12] J.M. Lopez-Villegas, A. Salas, N. Vidal, J. Sieiro, Study of 3D-printed helical-microstrip transmission lines, in: 2019 IEEE MTT-S International Microwave Symposium (IMS), (ISSN: 2576-7216) 2019, pp. 1221–1224.

[13] X. Chen, Z. Zhang, S. Yu, T. Zsurzsan, Fringing effect analysis of parallel plate capacitors for capacitive power transfer application, in: 2019 IEEE 4th International Future Energy Electronics Conference (IFEEC), 2019, pp. 1–5.

[14] B. Luo, R. Mai, Y. Chen, Y. Zhang, Z. He, A voltage stress optimization method of capacitive power transfer charging system, in: 2017 IEEE Applied Power Electronics Conference and Exposition (APEC), 2017, pp. 1456–1461.

[15] V. Hutson, The circular plate condenser at small separations, Math. Proc. Camb. Phil. Soc. 59 (1) (1963) 211–224, http://dx.doi.org/10.1017/S0305004100002152.

[16] G.J. Sloggett, N.G. Barton, S.J. Spencer, Fringing fields in disc capacitors, J. Phys. A: Math. Gen. 19 (14) (1986) 2725–2736, http://dx.doi.org/10.1088/0305-4470/19/14/012.

[17] L.Q. Hung, Compact 3 db wideband power divider for marine applications, in: 2020 International Multi-Conference on Industrial Engineering and Modern Technologies (FarEastCon), 2020, pp. 1–4, http://dx.doi.org/10.1109/FarEastCon50210.2020.9271360.

[18] D.A. Letavin, Compact branch-line coupler based on an inductor and a U-shaped capacitor, in: 2018 19th International Conference of Young Specialists on Micro/Nanotechnologies and Electron Devices (EDM), 2018, pp. 195–198, http://dx.doi.org/10.1109/EDM.2018.8435096.

[19] V.K. Velidi, A. Subramanyam, V. Senthil Kumar, Y. Mehta, S. Sanyal, Compact harmonic suppression branch-line coupler using signal-interference technique, in: 2016 Asia-Pacific Microwave Conference (APMC), 2016, pp. 1–4, http://dx.doi.org/10.1109/APMC.2016.7931397.

[20] S. Koziel, P. Kurgan, Low-cost optimization of compact branch-line couplers and its application to miniaturized butler matrix design, in: 2014 44th European Microwave Conference, 2014, pp. 227–230, http://dx.doi.org/10.1109/EuMC.2014.6986411.

[21] M. Kulkarni, A.N. Cheeran, K.P. Ray, S.S. Kakatkar, Novel compact implementation of rat-race hybrid coupler using coaxial cable for VHF applications, in: 2019 TEQIP III Sponsored International Conference on Microwave Integrated Circuits, Photonics and Wireless Networks (IMICPW), 2019, pp. 69–71, http://dx.doi.org/10.1109/IMICPW.2019.8933215.

A. Salas-Barenys received the B.E. degree in electronics engineering of telecommunication from the University of Barcelona (UB), Barcelona, Spain, and the M.S. degree in telecommunication engineering from the Universitat Autònoma de Barcelona (UAB), Barcelona, in 2017. He is currently pursuing the Ph.D. degree in engineering and applied science at UB. His current research interests include electronics design, radio frequency and electromagnetic modeling, communication systems, 3-D design, and 3-D printing.

N. Vidal received the Ph.D. degree in physics from the University of Barcelona, Barcelona, Spain, in 1995. She is currently an Associate Professor with the University of Barcelona, where she is also a member of the Group of Excellence for Radio Frequency Components and Systems. Her current research interests include antenna design for biomedical applications and electromagnetic propagation-related issues.

J.M. López-Villegas(M93SM03) received the Ph.D. degree in physics from the University of Barcelona, Barcelona, Spain, in 1990. He is currently the Director of the Group of Excellence for Radio Frequency Components and Systems, University of Barcelona, where he is also a Full Professor with the Department of Electronic and Biomedical Engineering. His current research interests include the design, optimization, and test of RF components, circuits, and systems performed using silicon, multilayered technologies, like multi-chip modules and low-temperature co-fired ceramics, 3-D printing, especially modeling and optimization of integrated inductors and transformers for general RF applications, development of new homodyne transceiver architectures based on injection-locked oscillators, the use of 3-D simulators for electro-magnetic analysis of RF components, circuits and systems, the analysis of electromagnetic compatibility and electromagnetic interference problems, and the interaction of electromagnetic energy with biological tissues.